Temperature thresholds of ecosystem respiration at a global scale.

Article

Accepted Version

Johnston, A. S. A. ORCID: https://orcid.org/0000-0001-8781-4039, Meade, A. ORCID: https://orcid.org/0000-0001-7095-7711, Ardö, J. ORCID: https://orcid.org/0000-0002-9318-0973, Arriga, N. ORCID: https://orcid.org/0000-0001-5321-3497, Black, A., Blanken, P. D. ORCID: https://orcid.org/0000-0002-7405-2220, Bonal, D. ORCID: https://orcid.org/0000-0001-9602-8603, Brümmer, C. ORCID: https://orcid.org/0000-0001-6621-5010, Cescatti, A., Dušek, J. ORCID: https://orcid.org/0000-0001-6119-0838, Graf, A. ORCID: https://orcid.org/0000-0003-4870-7622, Gioli, B. ORCID: https://orcid.org/0000-0001-7631-2623, Goded, I. ORCID: https://orcid.org/0000-0002-1912-325X, Gough, C. M. ORCID: https://orcid.org/0000-0002-1227-7731, Ikawa, H., Jassal, R. ORCID: https://orcid.org/0000-0002-6727-5215, Kobayashi, H. ORCID: https://orcid.org/0000-0001-9319-0621, Magliulo, V. ORCID: https://orcid.org/0000-0001-5505-6552, Manca, G. ORCID: https://orcid.org/0000-0002-9376-0310, Montagnani, L. ORCID: https://orcid.org/0000-0003-2957-9071, Moyano, F. E. ORCID: https://orcid.org/0000-0002-4090-5838, Olesen, J. E. ORCID: https://orcid.org/0000-0002-6639-1273, Sachs, T. ORCID: https://orcid.org/0000-0002-9959-4771, Shao, C., Tagesson, T. ORCID: https://orcid.org/0000-0003-3011-1775, Wohlfahrt, G. ORCID: https://orcid.org/0000-0003-3080-6702, Wolf, S. ORCID: https://orcid.org/0000-0001-7717-6993,

1 **Temperature thresholds of ecosystem respiration at a global scale**

2 Alice S.A. Johnston[1,2]*, Andrew Meade[2], Jonas Ardö[3], Nicola Arriga[4], Andy Black[5], Peter D.

3 Blanken[6], Damien Bonal[7], Christian Brümmer[8], Alessandro Cescatti[4], Jiří Dušek[9], Alexander

4 Graf[10], Beniamino Gioli[11], Ignacio Goded[4], Christopher M. Gough[12], Hiroki Ikawa[13], Rachhpal

5 Jassal[5], Hideki Kobayashi[14], Vincenzo Magliulo[15], Giovanni Manca[4], Leonardo

6 Montagnani[16,17], Fernando E. Moyano[18], Jørgen E. Olesen[19], Torsten Sachs[20], Changliang

7 Shao[21], Torbern Tagesson[22], Georg Wohlfahrt[23], Sebastian Wolf[24], William Woodgate[25,26],

8 Andrej Varlagin[27], Chris Venditti[2]

9 [1] School of Water, Energy and Environment, Cranfield University, Bedfordshire, MK43 0AL, UK.

10 [2] School of Biological Sciences, University of Reading, Reading, RG6 6BX, UK.

11 [3] Physical Geography and Ecosystem Science, Lund University Sölvegatan 12, Sweden.

12 [4] European Commission, Joint Research Centre (JRC), Ispra, Italy.

13 [5] Faculty of Land and Food Systems; University of British Columbia; Vancouver, BC V6T 1Z4, Canada.

14 [6] Department of Geography, University of Colorado, Boulder CO, USA 80309-0260.

15 [7] Université de Lorraine, AgroParisTech, INRAE, UMR Silva, 54000 Nancy, France.

16 [8] Thünen Institute of Climate-Smart Agriculture, Bundesallee 65, 38116 Braunschweig, Germany.

17 [9] Global Change Research Institute of the Czech Academy of Sciences, CZ-60300 Brno, Czech Republic.

18 [10] Forschungszentrum Jülich, Institute for Bio- and Geosciences 3: Agrosphere, 52080 Jülich, Germany.

19 [11] CNR, Institute of Bioeconomy, 50145 Firenze, Italy.

20 [12] Virginia Commonwealth University, Department of Biology, Richmond, VA 23234, USA

21 [13] Institute for Agro-Environmental Sciences, National Agriculture and Food Research Organization, Tsukuba,

22 305-8604, Japan

23 [14] Research Institute for Global Change, Institute of Arctic Climate and Environment Research, Japan Agency for

24 Marine-Earth Science and Technology, Japan.

25 [15] CNR, Institute for Mediterranean Agriculture and Forest Systems, 85 80040 Ercolano, Italy.

26 [16] Autonomous Province of Bolzano, Forest Services, Bolzano 39100, Italy.

27 [17] Faculty of Science and Technology, Free University of Bolzano, Bolzano 39100, Italy

28 [18] University of Goettingen, Bioclimatology, Büsgenweg 2, 37077 Göttingen, Germany

29 [19] Aarhus University, Department of Agroecology, Blichers Allé 20, 8830 Tjele, Denmark

30 [20] GFZ German Research Centre for Geoscience, Telegrafenberg, Potsdam, Germany

31 [21] Institute of Agricultural Resources and Regional Planning, Chinese Academy of Agricultural Sciences, Beijing

32 100081, China.

33 [22] Department of Geosciences and Natural Resources, University of Copenhagen, Öster Voldgade 10,

34 Copenhagen, Denmark.

35 [23] Department of Ecology, University of Innsbruck, 6020 Innsbruck, Austria.

36 [24] Department of Environmental Systems Science, ETH Zurich, 8092 Zurich, Switzerland.

37 [25] Land & Water, Commonwealth Scientific and Industrial Research Organisation, 2601, Canberra, Australia

38 [26] School of Earth and Environmental Sciences, The University of Queensland, 4067, Queensland, Australia.

39 [27] A.N. Severtsov Institute of Ecology and Evolution, Russian Academy of Sciences, 119071, Leninsky pr.33,

40 Moscow, Russia

41 *Correspondence: a.s.johnston@cranfield.ac.uk

42 **Abstract**

43 Ecosystem respiration is a major component of the global terrestrial carbon cycle and is

44 strongly influenced by temperature. The global extent of the temperature-ecosystem

45 respiration relationship, however, has not been fully explored. Here, we test linear and

46 threshold models of ecosystem respiration across 210 globally distributed eddy covariance

47 sites covering the most extensive temperature range ever studied. We find thresholds to the

48 global temperature-ecosystem respiration relationship at high and low air temperatures and

49 mid soil temperatures, which represent transitions in the temperature dependence and

50 sensitivity of ecosystem respiration. Annual ecosystem respiration rates show a markedly

51 reduced temperature dependence and sensitivity compared to half-hourly rates, and a single

52 mid-temperature threshold for both air and soil temperature. Our study indicates a distinction

53 in the influence of environmental factors, including temperature, on ecosystem respiration

54 between latitudinal and climate gradients at short (half-hourly) and long (annual) timescales.

55 Such climatological differences in the temperature sensitivity of ecosystem respiration have

56 important consequences for the terrestrial net carbon sink under ongoing climate change.

57 **Main**

58 Carbon losses from terrestrial ecosystems determine the direction and magnitude of carbon-

59 climate feedbacks[1,2]. The trajectory of future climate change therefore depends on the

60 biological processes that underpin ecosystem fluxes. Ecosystem respiration (R_e), the

61 cumulative respiration of autotrophs (plants) and heterotrophs (bacteria, fungi and animals),

62 represents a major component of the global carbon cycle[3]. Temperature strongly influences

63 R_e through the laws of thermodynamics[4–6], but the global extent of the temperature-R_e

64 relationship has not been fully explored[7,8].

65 Temperature-mediated variations in R_e are typically described as an exponential function in

66 Earth system models (ESMs)[2]. That is, globally static Q_{10} values of around 2 represent a

67 doubling of ecosystem CO_2 fluxes with an increase in temperature of 10 °C, when all other

68 terms are equal[9]. Empirical and theoretical studies, however, have documented conflicting

69 temperature-R_e relationships. Latitudinal shifts in the temperature sensitivity of R_e have been

70 observed in empirical studies, with ecosystems experiencing greater increases in R_e with

71 temperature at high, compared to mid and low, latitudes[8,10,11]. At the same time, global

72 syntheses have proposed convergent temperature sensitivities of R_e across different

73 climates and ecosystem types[4,12,13].

74 The influence of temperature on ecosystem respiration is mediated by the temperature

75 sensitivity of individual physiology, community composition and biotic interactions of all the

76 organisms inhabiting an ecosystem[13,14]. At the individual-level, metabolic rates scale with

77 body mass and increase exponentially with temperature according to the Boltzmann factor,

78 $e^{-E/kT}$, where E is the activation energy (eV), k is the Boltzmann's constant (8.62×10^{-5} eV

79 K^{-1}), and T is temperature (in Kelvin)[6]. Widescale application of the Boltzmann factor to

80 individual metabolic rates has revealed a common value of E between 0.6 and 0.7 eV[5,6,15]. At

81 the ecosystem-level, models based on metabolic theory indicate exponential temperature-R_e

82 relationships across diverse ecosystems with a value of E surprisingly similar to individual

83 metabolic rates (0.65 eV; $Q_{10} \sim 2.50$[4,13]). Yet, models of the temperature-R_e relationship have

84 focused on a limited temperature range between 0 and 30 °C, even though terrestrial

85 ecosystems experience temperatures between -60 and 50 °C[16].

86 In this study we test the generality of the temperature-R_e relationship, described by a general

87 ecosystem model, across the most extensive temperature range yet investigated. The

88 model, founded in metabolic theory, gives the linear expression:

89 $$\ln(R_e) = \frac{-E}{1{,}000k}\left(\frac{1{,}000}{T}\right) + \ln[(b_0)(C)] \tag{1}$$

90 where $\ln(R_e)$ is the natural logarithm of ecosystem respiration, in W ha^{-1}; $(1{,}000/T)$ is the

91 reciprocal of absolute temperature; b_0 is the intensity of cellular metabolism; and C is the

92 size distribution of organisms (assumed to be independent of R_e according to the energy

93 equivalence rule)[4]. The model predicts a general linear relationship between $(1{,}000/T)$ and

94 $\ln(R_e)$, with an expected slope ($\bar{E}$ from hereon in) across diverse ecosystems equal to -7.50

95 K (0.65 eV, with a plausible range between -2 and -11 K, or 0.2 and 1.2 eV)[10]. However, we

96 would expect climatological differences in resource supply[17,18] and community

97 composition[14,19] to alter $\bar{E}$ across the global temperature range. We would also expect

98 divergent relationships between metabolism and resource supply with temperature to modify

99 the temperature-R_e relationship over time[13,20].

Results

101 We test the global extent of the linear temperature-R_e relationship predicted by metabolic

102 theory, by applying the model presented in Eq. 1 to measurements across 210 globally

103 distributed FLUXNET sites[21] (Figure 1 and Supplementary Data 1). Both short-term (half-

104 hourly) and long-term (annual) measurements were tested for air and soil temperature. The

105 half-hourly FLUXNET dataset is presented with more conventional temperature and R_e units

106 in Extended Data 1. The linear model (Eq. 1) was compared to a threshold model, which

107 accounts for variations in the activation energy ($\bar{E}$) in Eq. 1 above and below specified

108 temperature breakpoints (see Methods). That is, the threshold model accounts for shifts in

109 the temperature sensitivity of R_e across the global temperature range, and explains

110 latitudinal shifts in the temperature-R_e relationship observed in empirical studies[8,10,11]. All

111 models were linear mixed effects models and goodness of fit comparisons used Akaike

112 Information Criterion (AIC) measurements.

113 **Figure 1**

114 The threshold model, which integrated two temperature breakpoints of -24.8 ±0.15 and 15.1

115 ±0.22 °C, better explained R_e rates over the global extent of air temperatures in the

116 FLUXNET dataset than the linear model (ΔAIC = 3,839,265, Figure 2). Similar to previous

117 findings[4,13], the threshold model indicates a temperature sensitivity of R_e indistinguishable

118 from that of -7.50 K (0.65 eV, dashed line in Figs. 2a & b) predicted by metabolic theory

119 (likelihood ratio test: χ^2 = 0, p = 1) between temperature breakpoints ($\bar{E}$ = -7.42 K, 0.64 eV,

120 Q_{10} ~ 2.45 between 15.1 and -24.8 °C, solid line in Fig. 2b). Evaluation of the linear model,

121 on the other hand, gives an activation energy for global R_e rates of -7.30 K (0.63 eV, solid

122 lines in Fig. 2a), significantly different from that predicted by metabolic theory (likelihood ratio

123 test: χ^2 = 20009, p < 0.0001). Importantly, the threshold model indicates a lower temperature

124 sensitivity of R_e at higher temperatures ($\bar{E}$ = -2.84 K, 0.25 eV, Q_{10} ~ 1.41 above 15.1 °C) and

125 extreme temperature sensitivity of R_e at very low temperatures ($\bar{E}$ = -30.53 K, 2.64 eV, Q_{10} ~

126 40.79 below -24.8 °C). The threshold model therefore primarily improves predictions,

127 compared to the linear model, of the temperature-R_e relationship at low and high latitude

128 sites (Figs. 2f & g). High measured variability in R_e across the global temperature range,

129 however, likely reflects the interactive effects of disturbance events, plant phenology and soil

130 water and nutrient limitation on ecosystem metabolism.

131 **Figure 2**

132 Given the importance of belowground communities in R_e[14,19], linear and threshold models

133 were tested for the global relationship between soil temperature and ecosystem respiration

134 (Figure 2 and Supplementary Table 2). A single temperature threshold of 11.4 ±0.29 °C

135 emerged for soil temperature, with little evidence for a lower temperature breakpoint

136 (likelihood ratio test: χ^2 = 0, p = 1). Above the temperature threshold, the activation energy of

137 R_e was lower than that observed for air temperature ($\bar{E}$ = -2.18 K, 0.19 eV, Q_{10} ~ 1.30), while

138 below the temperature threshold the activation energy was steeper than that between air

139 temperature thresholds ($\bar{E}$ = -13.37 K, 1.16 eV, Q_{10} ~ 5.05). The absence of a lower

140 threshold for R_e with soil temperature is likely explained by thermal insulation from snow

141 cover at low temperatures[22] resulting in much fewer observations, compared to air

142 temperature, of the soil temperature-R_e relationship below 0 °C.

143 To account for the relative uncertainties of eddy covariance measurements below -20 °C[23],

144 alongside the emergence of a single temperature breakpoint for soil temperature, we tested

145 the sensitivity of the air temperature threshold model to temperature ranges with few

4

146 available measurements (Extended Data 2). Ecosystem respiration data were classified in 5

147 °C temperature intervals and intervals containing < 1% of all measurements (n < 235,521)

148 were defined as low frequency intervals. Such intervals were present at both high (> 36 °C)

149 and low (< -19 °C) temperatures. Each low frequency temperature interval was removed one

150 by one, as well as all together (~ 1.8 % of the dataset), to investigate the sensitivity of the

151 threshold model. The test provides supporting evidence of the robustness of temperature

152 breakpoints to the removal of each temperature interval one by one. However, there was no

153 support for a lower temperature breakpoint (-24.8 °C in Fig. 2b & c) when all low frequency

154 intervals or all those < -19 °C were removed. Instead, a single temperature breakpoint of

155 14.6 °C emerged (Extended Data 3 and Supplementary Table 3). The lower air temperature

156 breakpoint should therefore be considered with caution until more accurate R_e

157 measurements at low temperatures can be made. R_e rates nevertheless display a sharp

158 decline at lower temperatures for both air (Fig. 2b) and soil (Fig. 3b) temperatures.

159 **Figure 3**

160 Sharp declines in R_e at low soil and air temperatures likely indicate pulse responses of soil

161 respiration to rewetting and thawing events[24], attributed to the suppression of microbial

162 activity under water limitation in freezing conditions[25] and an uncoupling of the temperature

163 dependence of microbial respiration from thermodynamic laws[26]. Differences between global

164 temperature-R_e relationships for air and soil temperature at short timescales also suggest

165 shifts in the contribution of aboveground and belowground communities to R_e across the

166 global extent of temperatures. For instance, a lower activation energy for the temperature-R_e

167 relationship at higher soil temperatures ($\bar{E}$ = -2.18 K > 11.4 ±0.29 °C, Fig. 3), compared to air

168 temperatures ($\bar{E}$ = -2.84 K > 15.1 °C, Fig. 2), could indicate a relative reduction in the

169 contribution of belowground autotrophs and heterotrophs to R_e in warmer climates. On the

170 other hand, the lower threshold for the temperature-R_e relationship at low air temperatures

171 could reflect a temperature limit for the metabolism of aboveground communities, whereas

172 the absence of a lower temperature threshold for soil temperature suggests the importance

173 of belowground communities as components of R_e in mild to cold climates.

174 Global air temperature thresholds were consistent across climates, but the goodness of fit of

175 the threshold model (pseudo r^2 and ΔAICs compared to the linear model, Fig. 4) declined

176 with a decrease in overall temperature range at lower latitudes. For instance, the

177 temperature dependence of R_e (variation in R_e rates explained by temperature) was greater

178 in cold, higher latitude, climates (tundra and boreal, r^2_m > 0.60), compared to mild

179 (temperate, r^2_m = 0.48) and warm, low latitude, climates (mediterranean and tropical, r^2_m ≤

180 0.09). In warmer climates, random effects had a much greater influence on R_e than in mild or

181 cold climates, with FLUXNET site and latitude explaining more variation in tropical and

182　　mediterranean ecosystems (Supplementary Table 4). Across the 210 sites, the threshold

183　　model better predicted the temperature-R_e relationship in the majority of cases (n = 197,

184　　Supplementary Data 1), while temperature explained more of the variation in R_e rates at

185　　sites with greater temperature ranges and higher latitudes (and Extended Data 4).

186　　Q_{10} estimates from the threshold model reflect latitudinal shifts in the temperature sensitivity

187　　of ecosystem respiration, with tropical, mediterranean, temperate, boreal, and tundra

188　　climates yielding Q_{10} values of 1.38 ±0.01, 1.82 ±0.43, 2.32 ±0.31, 2.67 ±0.10, and 2.90

189　　±0.12 respectively, compared to a global Q_{10} of 2.26 ±0.35, and higher Q_{10} estimates based

190　　on the soil temperature threshold model (Supplementary Table 5). Empirical observations of

191　　R_e, soil respiration and carbon turnover rates are comparable with threshold model

192　　estimates of higher temperature sensitivities of R_e at high-latitudes and lower temperature

193　　sensitivities of R_e at low-latitudes[10,27]. Weaker temperature control in the linear model, similar

194　　to ESMs that implement static global Q_{10} values, cannot capture shifts in R_e temperature

195　　sensitivities across the global temperature range (Supplementary Table 5).

196　　**Figure 4**

197　　Annual temperature-R_e relationships were analysed across site years to investigate whether

198　　climatological differences in the temperature dependence and sensitivity of R_e emerge over

199　　longer timescales. The threshold model explained the temperature-R_e relationship better

200　　than the linear model at longer timescales for both air and soil temperature (Fig. 5).

201　　Surprisingly, threshold models converged for air and soil temperature, with a single mid-

202　　temperature breakpoint of 11.0 ±0.16 °C (Figs 5b & d). Above the temperature threshold,

203　　annual R_e rates declined with increasing mean annual temperatures from mid to low

204　　latitudes, while the activation energy below the temperature threshold was markedly reduced

205　　(Figs 5a & c, $\bar{E}$ ~ -4.90 K, 0.42 eV) compared to short timescales. Weaker temperature

206　　relationships at longer timescales is reflected by global Q_{10} estimates of 1.34 ±0.55 and 1.29

207　　±0.58 for air and soil temperature, respectively (Supplementary Table 6). An overall lack of

208　　R_e variation explained by temperature (r^2_m < 0.14) likely reflects the importance of

209　　confounding effects from soil water, nutrient limitation, and resource availability, alongside

210　　thermal acclimation, at longer timescales. The threshold model was further consistent for

211　　annual soil respiration and air temperature measurements from the Global Soil Respiration

212　　Database[28], with a single temperature breakpoint of 5.5 °C (Extended Data 5 and

213　　Supplementary Table 6).

214　　**Figure 5**

215

Discussion

Our study shows how latitudinal shifts in R_e temperature sensitivity at both short and long timescales correspond to transitions in the global temperature–R_e relationship across temperature thresholds. Importantly, temperature thresholds also indicate differences in the temperature dependence of R_e, with more variation in R_e rates explained by temperature in cold compared to warm climates. In cold climates, temperature strongly influences metabolic activity of belowground microbial communities[19,25,26]. In warm climates, ecosystem metabolism is limited by water and nutrient availability, and resource availability to biological communities[18,27,29–31].

Both the temperature sensitivity and dependence of annual R_e rates is markedly reduced compared to the short-term R_e temperature response, suggesting the dominance of resource effects on ecosystem metabolism at longer timescales[13]. For instance, primary production directs carbon availability for ecosystem metabolism and typically shows a weaker temperature dependence[20,32]. Nutrient availability further drives preferential allocation of photosynthate C above- or below-ground, with consequences for carbon availability and quality to different ecosystem components[17].

Thresholds to the temperature-R_e relationship shown here will undoubtedly result from temporally divergent sensitivities between ecosystem components (e.g. below- and above-ground, heterotrophic and autotrophic) and several environmental controls over time. Variable acclimation of the different components of R_e to these environmental controls may further influence the temperature dependence and sensitivity of R_e by modifying the temperature response of catabolic and anabolic pathways[33–35]. Although we would expect such mechanisms to occur as gradual state changes rather than the sharp breakpoints described here, our study indicates consistent temperature thresholds at which ecosystem metabolism changes at a global scale. However, such results need to be validated for different ecosystem components as detailed measurements become available, and for decadal timescales over which the influence of anthropogenic factors can be detected.

Biosphere feedbacks with future climate changes will be strongly influenced by the temperature-R_e relationship[36,37] and latitudinal shifts in R_e temperature sensitivity as identified here will have important consequences for the global net land carbon sink[38]. For instance, while huge stores of labile carbon in permafrost regions could be released if temperatures rise above lower thresholds for microbial decomposition[26], CO_2 fertilisation in tropical and boreal regions could enhance carbon gains through primary production relative to losses through R_e[30,39]. Climate change forecasts by ESMs would thus be improved by accounting for temperature thresholds of R_e at a global scale. A higher resolution

251 understanding of R_e-climate feedbacks, however, requires strategic disentangling of the

252 multiple environmental controls on the aboveground, belowground, heterotrophic, and

253 autotrophic components of terrestrial ecosystem carbon fluxes.

Methods

The FLUXNET dataset

256 FLUXNET is a global network of micrometeorological sites providing eddy covariance CO_2

257 exchange observations between terrestrial ecosystems and the atmosphere[21]. The

258 FLUXNET 2015 dataset used in this study provides half hourly temperature and night-time

259 R_e measurements over 1454 site years and a latitudinal range of 78.92 °N to 37.43 °S.

260 Observations across the 210 sites, which range from arctic tundra to tropical rainforest

261 ecosystems, provide an extensive temperature range of 89.7 °C, from -43.4 to 46.3 °C

262 (Figure 1 and Supplementary Data 1).

263 The FLUXNET dataset is subject to a data processing pipeline which include data quality

264 controls checks, filtering of low turbulence periods and partitioning of CO_2 fluxes into

265 respiration and photosynthesis components using established methods[21]. Disentangling

266 respiration and photosynthesis fluxes during the day is complex and the extraction of R_e

267 relies on modelling techniques with high uncertainty. Night-time CO_2 exchange

268 measurements thus provide the best approximation of R_e, and uncertainty has been

269 minimised for the FLUXNET dataset by employing quality control procedures[21]. Here, non-

270 gap-filled half hourly (µmol CO_2 m^{-2} s^{-1}) and annual (g C m^{-2}) night-time R_e

271 (RECO_NT_VUT_MEAN), air temperature (TA_F) and soil temperature (TS_F)

272 measurements were compiled from the FLUXNET 2015 dataset

273 (https://fluxnet.fluxdata.org/data/fluxnet2015-dataset/). R_e measurements were then

274 converted to units of metabolic energy (W ha^{-1})[4] by taking 0.272 J µmol CO_2 and 10,000 m^2

275 ha^{-1}.

Model analysis

277 The linear model (1) for describing the temperature-R_e relationship was fitted to the global

278 FLUXNET dataset, for both air and soil temperature. To test for the presence of temperature

279 thresholds to the linear temperature–R_e model at a global scale, which explain shifts in R_e

280 temperature sensitivity across climates, we compare the linear model in Eq. 1 to a threshold

281 (piecewise) model. The threshold model, with two temperature breakpoints, gives:

$$\ln(Re) = \bar{E}_1 f_1(1{,}000/T, k_1) + \bar{E}_2 f_2(1{,}000/T, k_1, k_2) \, k2) + \bar{E}_3 f_3(1{,}000/T, k_2) + \ln[(b_0)(C)] \quad (2)$$

283 where $\bar{E}_1$, $\bar{E}_2$ and $\bar{E}_3$ represent activation energies for different temperature ($1{,}000/T$) ranges,

284 determined by the two temperature breakpoints (k_1 and k_2) and f represents the functions:

285

286
$$f_1 = \begin{cases} 1{,}000/T, & 1{,}000/T \le k_1 \\ k_1, & k_1 > 1{,}000/T \end{cases}$$

287
$$f_2 = \begin{cases} 0, & 1{,}000/T \le k_1 \\ 1{,}000/T - k_1, & k_1 \le 1{,}000/T \le k_2 \\ k_2 - k_1, & 1{,}000/T > k_2 \end{cases}$$

288
$$f_3 = \begin{cases} 0, & 1{,}000/T \le k_2 \\ 1{,}000/T, & 1{,}000/T > k_2 \end{cases}$$

289 The threshold model first introduced a single temperature breakpoint to the linear model, so
290 that the activation energy ($\bar{E}$, with more negative values indicating higher temperature
291 sensitivity) varies above and below a specified temperature. Temperature breakpoints were
292 tested for the temperature ($1{,}000/T$) range between 3.1 and 4.4, for every increment of 0.001
293 (~0.07 °C). Differences in linear and threshold model AIC's were then compared for every
294 temperature breakpoint. The highest ΔAIC was taken as providing the most support for a
295 temperature breakpoint, as long as ΔAIC > 5 for additional degrees of freedom and $p < 0.05$
296 in a likelihood ratio test. Then, the threshold model integrated an additional temperature
297 breakpoint, taking the first temperature breakpoint with the greatest support as a fixed
298 value. Model AIC's for each second temperature breakpoint were compared to the single
299 threshold model and the second threshold was selected based on the highest ΔAIC given
300 the conditions outlined above. Temperature breakpoints were identified for short (half-hourly)
301 and long (annual) temperature-R_e relationships.

302 All models were linear mixed effects models, with FLUXNET site and latitude set as random
303 effects. First, the models were tested for the global dataset and then for broadly classified
304 climate zones (cold, mild, and warm) and climates (tundra, boreal, temperate,
305 mediterranean, and tropical). Some generalisations were necessary during climate
306 classification. For instance, alpine sites at mid-latitudes were classified as boreal climates
307 (Supplementary Data 1). Linear and threshold models were further tested for each
308 FLUXNET site. Finally, annual R_e rates were used to investigate changes in temperature
309 breakpoints, and linear and threshold model performance, at long timescales for air and soil
310 temperature. Long timescale models accounted for latitude and year as random effects.

311 **References**

312 1. Cao, M. & Woodward, F. I. Dynamic responses of terrestrial ecosystem carbon cycling to
313   global climate change. *Nature* **393**, 249–252 (1998).

9

314   2. Heimann, M. & Reichstein, M. Terrestrial ecosystem carbon dynamics and climate

315   feedbacks. *Nature* **451**, 289–292 (2008).

316   3. Allen, A. P., Gillooly, J. F. & Brown, J. H. Linking the global carbon cycle to individual

317   metabolism. *Funct. Ecol.* **19**, 202–213 (2005).

318   4. Enquist, B. J. *et al.* Scaling metabolism from organisms to ecosystems. *Nature* **423**,

319   639–642 (2003).

320   5. Gillooly, J. F., Brown, J. H., West, G. B., Savage, V. M. & Charnov, E. L. Effects of size

321   and temperature on metabolic rate. *Science* **293**, 2248–2251 (2001).

322   6. Brown, J. H., Gillooly, J. F., Allen, A. P., Savage, V. M. & West, G. B. Toward a

323   metabolic theory of ecology. *Ecology* **85**, 1771–1789 (2004).

324   7. Friedlingstein, P. *et al.* Uncertainties in CMIP5 climate projections due to carbon cycle

325   feedbacks. *J. Clim.* **27**, 511–526 (2014).

326   8. Davidson, E. A. & Janssens, I. A. Temperature sensitivity of soil carbon decomposition

327   and feedbacks to climate change. *Nature* **440**, 165–173 (2006).

328   9. Lenton, T., M. & Huntingford, C. Global terrestrial carbon storage and uncertainties in its

329   temperature sensitivity examined with a simple model. *Glob. Change Biol.* **9**, 1333–1352

330   (2003).

331   10. Song, B. *et al.* Divergent apparent temperature sensitivity of terrestrial ecosystem

332   respiration. *J. Plant Ecol.* **7**, 419–428 (2014).

333   11. Lloyd, J. & Taylor, J. A. On the temperature dependence of soil respiration. *Funct. Ecol.*

334   315–323 (1994).

335   12. Mahecha, M. D. *et al.* Global Convergence in the Temperature Sensitivity of Respiration

336   at Ecosystem Level. *Science* **329**, 838–840 (2010).

337   13. Yvon-Durocher, G. *et al.* Reconciling the temperature dependence of respiration across

338   timescales and ecosystem types. *Nature* **487**, 472–476 (2012).

339   14. Johnston, A. S. A. & Sibly, R. M. The influence of soil communities on the temperature

340   sensitivity of soil respiration. *Nat. Ecol. Evol.* **2**, 1597–1602 (2018).

341   15. Dell, A. I., Pawar, S. & Savage, V. M. Systematic variation in the temperature

342   dependence of physiological and ecological traits. *Proc. Natl. Acad. Sci.* **108**, 10591–

343   10596 (2011).

344   16. Buckley, L. B. & Huey, R. B. Temperature extremes: geographic patterns, recent

345   changes, and implications for organismal vulnerabilities. *Glob. Change Biol.* **22**, 3829–

346   3842 (2016).

347   17. Gill, A. L. & Finzi, A. C. Belowground carbon flux links biogeochemical cycles and

348   resource-use efficiency at the global scale. *Ecol. Lett.* **19**, 1419–1428 (2016).

349   18. Green, J. K. *et al.* Large influence of soil moisture on long-term terrestrial carbon uptake.

350   *Nature* **565**, 476–479 (2019).

351   19. Allison, S. D., Wallenstein, M. D. & Bradford, M. A. Soil-carbon response to warming

352   dependent on microbial physiology. *Nat. Geosci.* **3**, 336–340 (2010).

353   20. Michaletz, S. T., Cheng, D., Kerkhoff, A. J. & Enquist, B. J. Convergence of terrestrial

354   plant production across global climate gradients. *Nature* **512**, 39–43 (2014).

355   21. Pastorello, G. *et al.* The FLUXNET2015 dataset and the ONEFlux processing pipeline

356   for eddy covariance data. *Sci. Data* **7**, 225 (2020).

357   22. Monson, R. K. *et al.* Winter forest soil respiration controlled by climate and microbial

358   community composition. *Nature* **439**, 711–714 (2006).

359   23. Mauder, M. *et al.* A strategy for quality and uncertainty assessment of long-term eddy-

360   covariance measurements. *Agric. For. Meteorol.* **169**, 122–135 (2013).

361   24. Kim, D.-G., Vargas, R., Bond-Lamberty, B. & Turetsky, M. R. Effects of soil rewetting

362   and thawing on soil gas fluxes: a review of current literature and suggestions for future

363   research. *Biogeosciences* **9**, 2459–2483 (2012).

364   25. Du, E. *et al.* Winter soil respiration during soil-freezing process in a boreal forest in

365   Northeast China. *J. Plant Ecol.* **6**, 349–357 (2013).

366   26. Schuur, E. A. *et al.* Climate change and the permafrost carbon feedback. *Nature* **520**,

367   171–179 (2015).

368   27. Koven, C. D., Hugelius, G., Lawrence, D. M. & Wieder, W. R. Higher climatological

369   temperature sensitivity of soil carbon in cold than warm climates. *Nat. Clim. Change* **7**,

370   817–822 (2017).

371   28. Bond-Lamberty, B. P. & Thomson, A. M. A Global Database of Soil Respiration Data,

372   Version 4.0. *ORNL DAAC* (2018) doi:https://doi.org/10.3334/ORNLDAAC/1578.

373   29. Zhang, Z. *et al.* A temperature threshold to identify the driving climate forces of the

374   respiratory process in terrestrial ecosystems. *Eur. J. Soil Biol.* **89**, 1–8 (2018).

375   30. Yang, Y., Donohue, R. J., McVicar, T. R., Roderick, M. L. & Beck, H. E. Long-term CO2

376   fertilization increases vegetation productivity and has little effect on hydrological

377   partitioning in tropical rainforests. *J. Geophys. Res. Biogeosciences* **121**, 2125–2140

378   (2016).

379   31. Fleischer, K. *et al.* Amazon forest response to CO 2 fertilization dependent on plant

380   phosphorus acquisition. *Nat. Geosci.* **12**, 736–741 (2019).

381   32. Padfield, D. *et al.* Metabolic compensation constrains the temperature dependence of

382   gross primary production. *Ecol. Lett.* **20**, 1250–1260 (2017).

383   33. Atkin, O. K. & Tjoelker, M. G. Thermal acclimation and the dynamic response of plant

384   respiration to temperature. *Trends Plant Sci.* **8**, 343–351 (2003).

385   34. Huntingford, C. *et al.* Implications of improved representations of plant respiration in a

386   changing climate. *Nat. Commun.* **8**, 1602 (2017).

387   35. Niu, S. *et al.* Thermal optimality of net ecosystem exchange of carbon dioxide and

388   underlying mechanisms. *New Phytol.* **194**, 775–783 (2012).

389   36. Rind, D. The Consequences of Not Knowing Low- and High-Latitude Climate Sensitivity.

390   *Bull. Am. Meteorol. Soc.* **89**, 855–864 (2008).

391   37. Liu, Z. *et al.* Increased high-latitude photosynthetic carbon gain offset by respiration

392   carbon loss during an anomalous warm winter to spring transition. *Glob. Change Biol.*

393   **26**, 682–696 (2020).

394   38. Haverd, V. *et al.* Higher than expected CO2 fertilization inferred from leaf to global

395   observations. *Glob. Change Biol.* **26**, 2390–2402 (2020).

396   39. Tagesson, T. *et al.* Recent divergence in the contributions of tropical and boreal forests

397   to the terrestrial carbon sink. *Nat. Ecol. Evol.* **4**, 202–209 (2020).
398

399
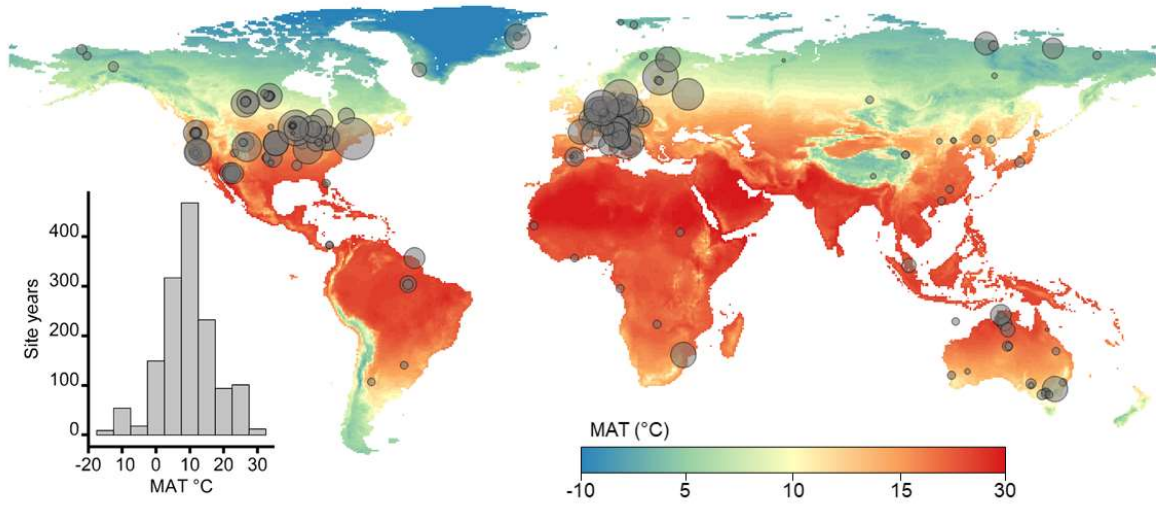
400   **Figure 1. Global distribution of the FLUXNET sites.** Site locations (n = 210) are displayed over a

401   world mean annual temperature (MAT) map. Symbol diameter represents the number of site years

402   (range: 1 to 22 years) and the inset left-hand figure shows the distribution of site years (n = 1454) by

403   MAT.

404
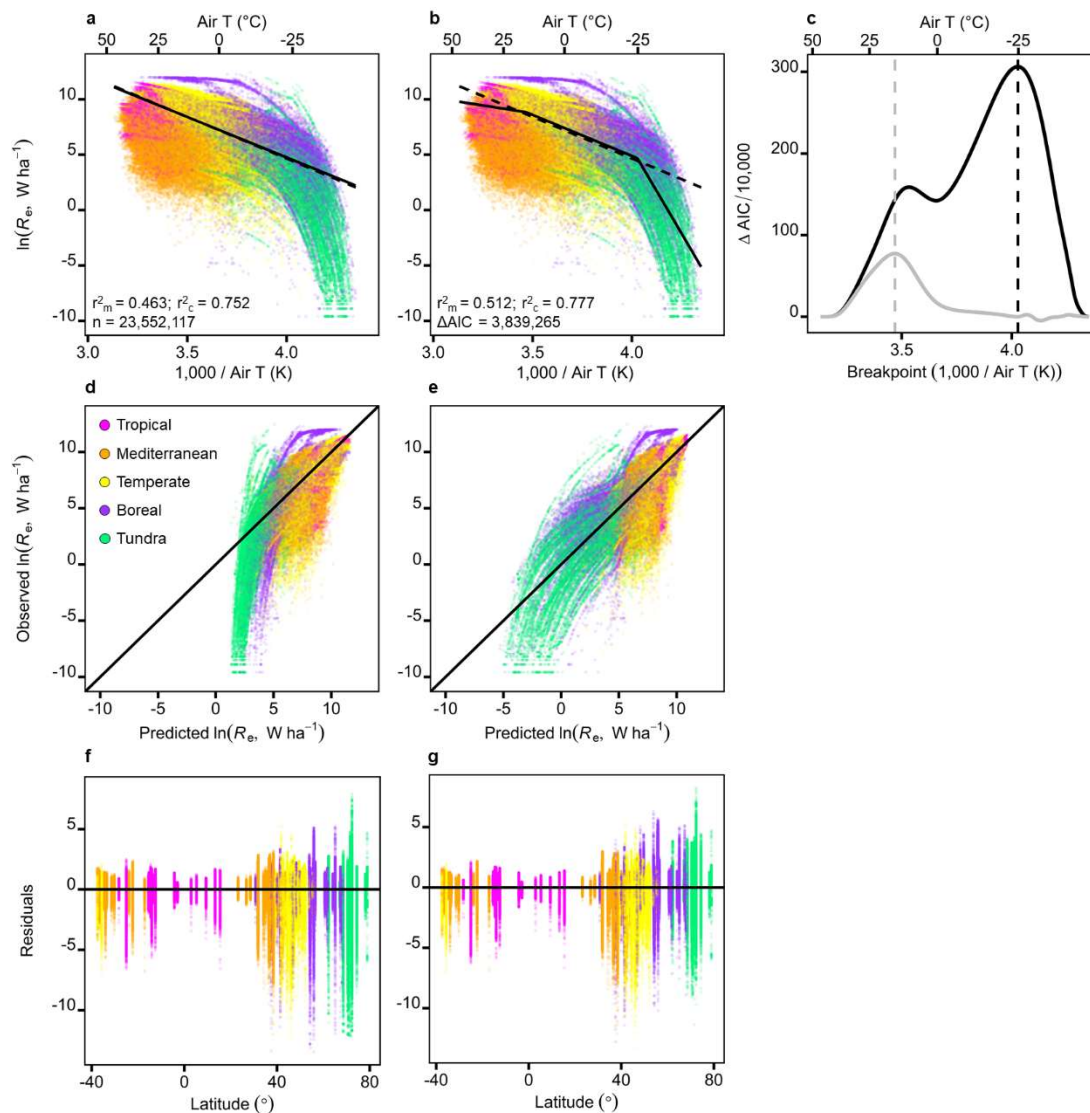
Figure 2. Global extent of the temperature-ecosystem respiration (R_e) relationship. Night-time half hourly ecosystem respiration measurements from the FLUXNET dataset (symbols), broadly classified as tropical (magenta), mediterranean (orange), temperate (yellow), boreal (purple) or tundra (green) climates. Left-hand plots (a, d & f) present predictions from the linear model (Eq. 1) and middle plots (b,e & g) from a threshold model with two temperature breakpoints (Eq. 2), of the temperature-ecosystem respiration relationship. The right-hand plot (c) shows the presence of two temperature breakpoints (black line: air ($1,000/T$)= 4.027, -24.8 °C; grey line: air ($1,000/T$) = 3.469, 15.1 °C), identified by the threshold models performance (ΔAIC's compared to the linear model where higher values provide a better fit to the FLUXNET dataset). Goodness of fit measures indicate the pseudo r^2 for marginal (fixed) effects (r^2_m) and conditional (fixed and random) effects (r^2_c), with top plots (a & b) showing predictions of the fixed effects only (temperature, solid lines) in each model compared to the activation energy of -7.50 K predicted by metabolic theory (dashed lines, r^2_m = 0.361; r^2_c = 0.542). Middle plots (d & e) present model predictions against observed FLUXNET measurements (solid black 1:1 lines would demonstrate perfect prediction), and bottom plots (f & g) show model residuals against latitude. Full details of the linear mixed effects models are presented in Supplementary Table 1.

14
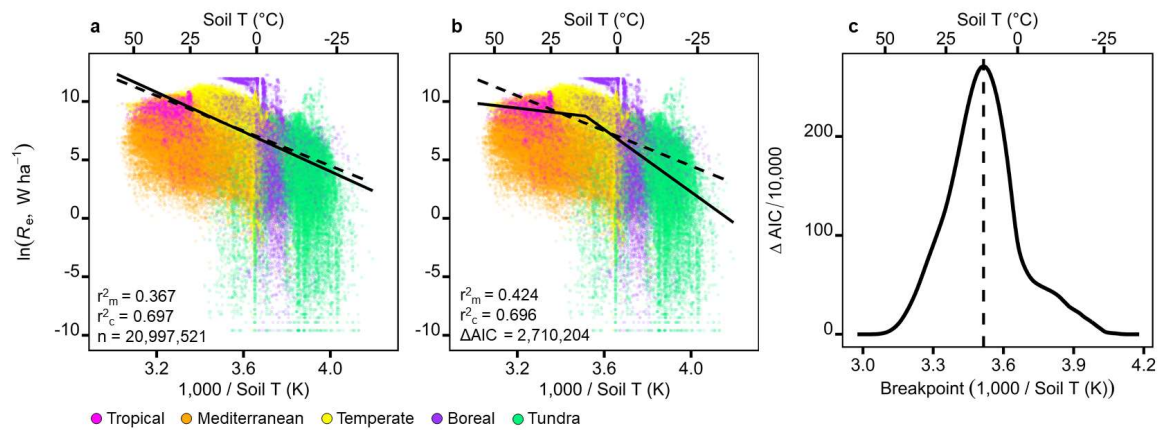
Figure 3. The global soil temperature-ecosystem respiration relationship. Night-time half hourly ecosystem respiration measurements from the FLUXNET dataset (symbols), broadly classified by climate with symbol colours as in Figure 2. Predictions of the temperature-ecosystem respiration relationship are compared for a) the linear model and b) the threshold model, for the fixed effects of temperature (solid lines). Both models are compared to the activation energy of -7.50 K predicted by metabolic theory (dashed lines, r^2_m = 0.173, r^2_c = 0.500). The right-hand plot (c) shows the presence of a single temperature breakpoints (black line: soil $(1,000/T)$ = 3.515, 11.4 °C), identified by the threshold models performance (ΔAIC's compared to the linear model where higher values provide a better fit to the FLUXNET dataset). Full details of the linear mixed effects models are presented in Supplementary Table 2.

15

434
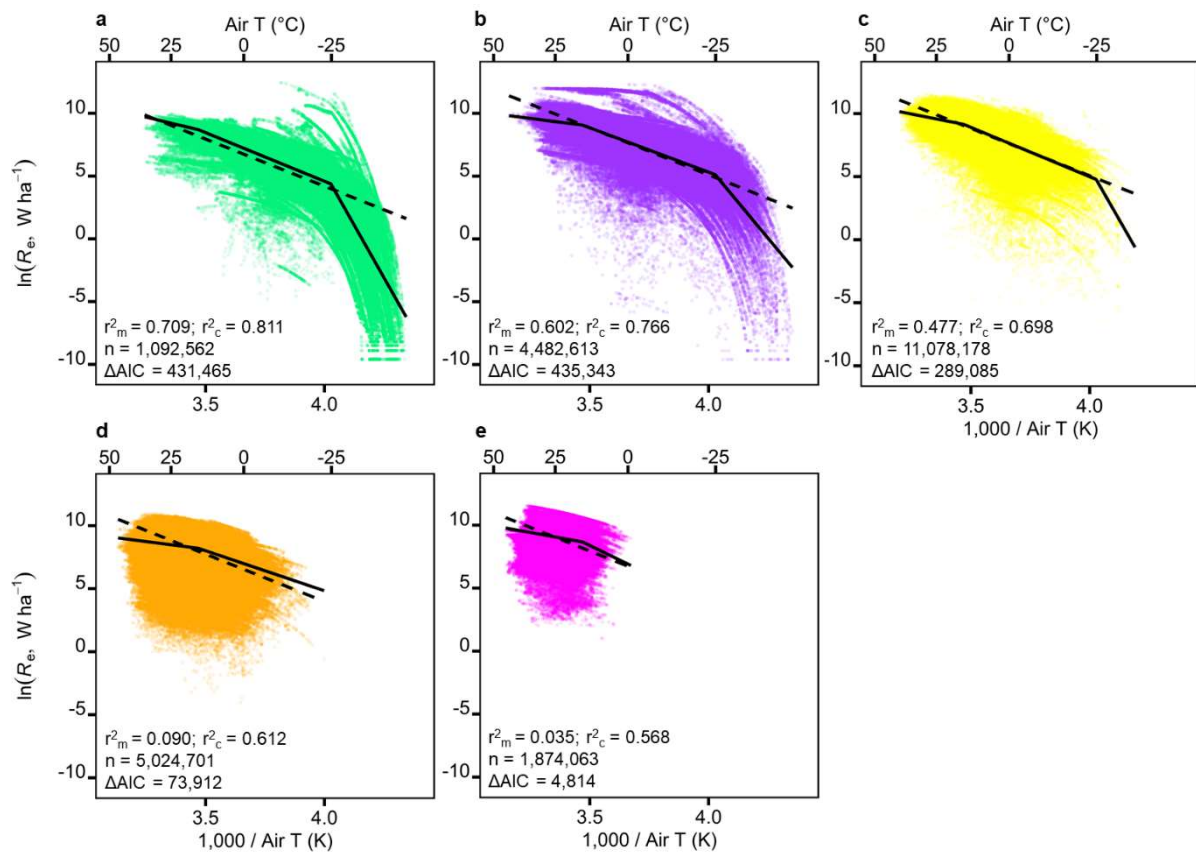
Figure 4. Temperature thresholds of ecosystem respiration (R_e) across five climates. Night-time half hourly ecosystem respiration measurements from the FLUXNET dataset (symbols), classified as a) tundra, b) boreal), c) temperate, d) mediterranean, and e) tropical, with symbol colours as in Figure 2. Solid lines show threshold model predictions for the fixed effects of temperature, and dashed lines show an activation energy of -7.5 K predicted by metabolic theory. ΔAICs indicate a greater goodness of fit of the threshold compared to linear model. Full details of the linear mixed effects models are presented in Supplementary Table 4.

442
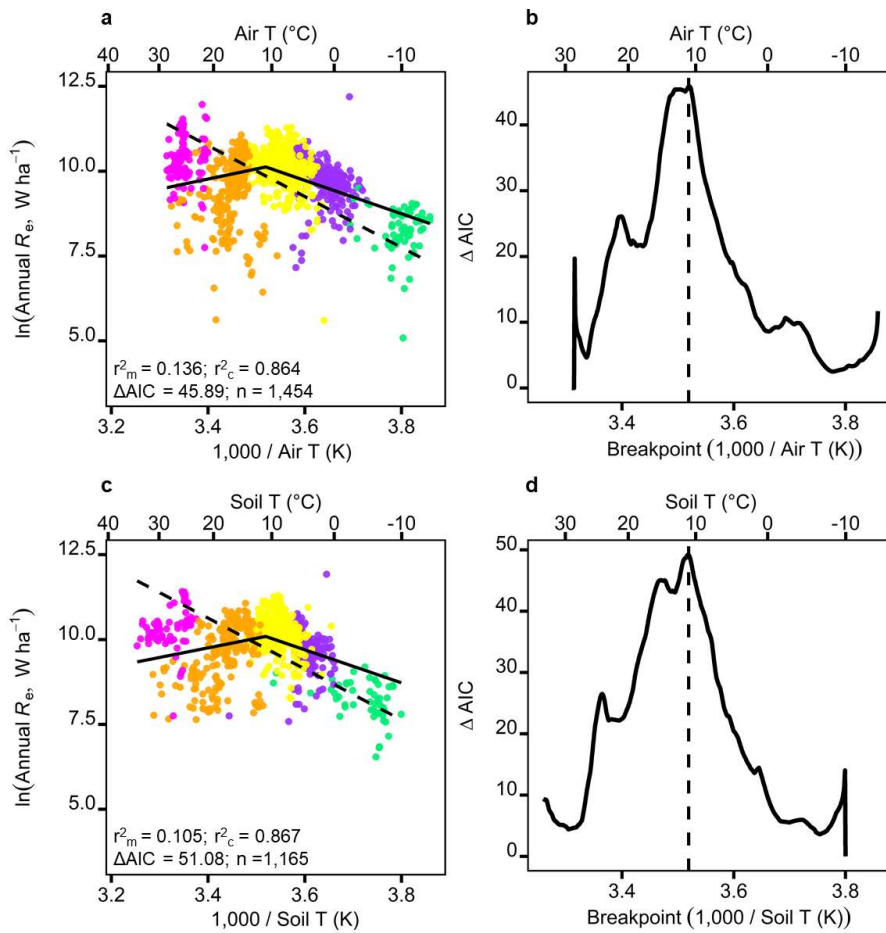
Figure 5. Long-term temperature thresholds of ecosystem respiration (R_e). Mean annual R_e and either a) air or c) soil temperature measurements (symbols), with symbol colours representing climate as in Figure 2. Plots show predictions from the threshold model (solid lines, for the fixed effects of temperature only). Both threshold models identified a single temperature breakpoint of 11.0 °C, with little support for a second temperature breakpoint (ΔAIC < 5 and p > 0.05). Dashed lines indicate an activation energy of -7.50 K as predicted by metabolic theory and ΔAICs are between the linear and threshold models. Full details of the threshold mixed effects models are presented in Supplementary Table 6.

Data availability

The dataset analysed during the current study is available on Dryad (https://doi.org/10.5061/dryad.70rxwdbwk).

Code availability

The R code used for analysis during the current study is available on Dryad (https://doi.org/10.5061/dryad.70rxwdbwk).

Author contributions

ASAJ and CV developed the methodology and led the writing of the manuscript. ASAJ and AM conduced the data analysis. JA, NA, DB, AB, PDB, CB, AC, JD, AG, BG, IG, CMG, HI, RJ, HK, VM, GM, LM, FEM, JEO, TS, CS, TT, GW, SW, WW, and AV contributed data. All authors contributed to manuscript revisions.

Competing interests

The authors declare no competing interests.